

This article was downloaded by: [Cerato, Amy]

On: 25 August 2010

Access details: Access Details: [subscription number 925054451]

Publisher Taylor & Francis

Informa Ltd Registered in England and Wales Registered Number: 1072954 Registered office: Mortimer House, 37-41 Mortimer Street, London W1T 3JH, UK



International Journal of Pavement Engineering

Publication details, including instructions for authors and subscription information:

<http://www.informaworld.com/smpp/title~content=t713646742>

Modelling the scale effect of granular media for strength and bearing capacity

Ching S. Chang^a; Amy B. Cerato^b; Alan J. Lutenecker^a

^a Department of Civil and Environmental Engineering, University of Massachusetts, Amherst, MA, USA ^b Department of Civil Engineering and Environmental Science, University of Oklahoma, Norman, OK, USA

Online publication date: 02 August 2010

To cite this Article Chang, Ching S. , Cerato, Amy B. and Lutenecker, Alan J.(2010) 'Modelling the scale effect of granular media for strength and bearing capacity', International Journal of Pavement Engineering, 11: 5, 343 – 353

To link to this Article: DOI: 10.1080/10298436.2010.488736

URL: <http://dx.doi.org/10.1080/10298436.2010.488736>

PLEASE SCROLL DOWN FOR ARTICLE

Full terms and conditions of use: <http://www.informaworld.com/terms-and-conditions-of-access.pdf>

This article may be used for research, teaching and private study purposes. Any substantial or systematic reproduction, re-distribution, re-selling, loan or sub-licensing, systematic supply or distribution in any form to anyone is expressly forbidden.

The publisher does not give any warranty express or implied or make any representation that the contents will be complete or accurate or up to date. The accuracy of any instructions, formulae and drug doses should be independently verified with primary sources. The publisher shall not be liable for any loss, actions, claims, proceedings, demand or costs or damages whatsoever or howsoever caused arising directly or indirectly in connection with or arising out of the use of this material.

Modelling the scale effect of granular media for strength and bearing capacity

Ching S. Chang^{a*}, Amy B. Cerato^b and Alan J. Lutenecker^a

^aDepartment of Civil and Environmental Engineering, University of Massachusetts, Amherst, MA 01002, USA;

^bDepartment of Civil Engineering and Environmental Science, University of Oklahoma, Norman, OK 73019, USA

(Received 4 February 2010; final version received 20 April 2010)

This paper investigates a method of analysis for the scale effect on shear strength of sands – a fundamental problem of considerable importance to soil mechanics. The phenomena of scale effect for direct shear box tests and footing bearing capacity tests are briefly described and the available analytical methods are discussed. First, the couple-stress theory is reviewed and its extension to a Drucker–Prager type is illustrated. Subsequently, material constants are discussed. Attention is then focused on the *internal length* of sand, which is shown to be the key parameter for scale effect for granular soil. Then, the predicted results are compared with experimental results on two sands. The main observations of the comparison for the scale effect are sketched and its limitations are discussed.

Keywords: scale effect; granular material; couple stress; shear strength; direct shear; bearing capacity

1. Introduction

Scale effects occur in many types of material. Metals display size dependence when deformed non-uniformly into the plastic range (Hutchinson 2000). The scale effect has also been found in torsion of copper and nickel wire (Fleck *et al.* 1994), and in the indentation of alloy plates (Atkinson 1995, Ma and Clarke 1995, Poole *et al.* 1996). Scale effects also exhibit in composite material, concrete and rock (Bandis 1979, Hudson 1993, Bazant 2000).

In granular soils, scale effects have been experimentally observed in the bearing capacity measured from footing tests (Berry 1935, DeBeer 1965, Tatsuoka *et al.* 1991) and in the shear strength measured from direct shear box tests. In general, the friction angles observed from experimental results are significantly higher for smaller footings and for smaller laboratory specimens.

Classic continuum mechanics do not have the capability of describing the effect of scale. Recently, new analytical models have been developed, that involve the concept of ‘internal length’, which now makes it possible to simulate the scale effect for granular soils. The studies of internal length, however, were predominantly performed for the formation and thickness of shear bands; very few studies have focused on the influence of internal length on scale effect, particularly compared with experimental measurements.

In this paper, we use an elastic–plastic model of couple-stress type to analyse the experimental results performed on two different sands. We attempt to study the factors influencing ‘internal length’ and the appropriate

range of internal length to be used for real granular soil. We also compare the analytical results with those of classic methods of analysis.

2. Scale effect

The scale effects examined in this paper are focused on those observed from direct shear box tests and from footing bearing capacity tests. Direct shear test is readily available in soil testing facilities and is commonly used by geotechnical engineers. The shear strength τ and the confining pressure σ are obtained, respectively, by dividing the forces F_h and F_v by the area of the specimen (see Figure 1(a)). The friction angle is estimated by the ratio $\tau/\sigma = \tan \phi$, which assumes that the horizontal plane through the shear box is the theoretical failure plane (Hansen 1961).

Intuitively, the shear strength should be independent of specimen size. However, Parsons (1936) demonstrated the opposite by showing experimental results for crushed quartz and for clean Ottawa sand tested in different shear box sizes. Results from both materials show that the friction angle decreases with increasing box size. The angle of the crushed quartz decreased from 31.5 to 30.7° and of the clean sand decreased from 31.0 to 28.5°.

More recently, Hight and Leroueil (2003) presented test results of dense Leighton Buzzard sand in different shear box sizes. They presented their results as the ratio of shear stress to normal stress versus the aspect ratio, H/L and showed that as the aspect ratio increased, the friction angle increased (see Figure 2). The results also showed

*Corresponding author. Email: chang@ecs.umass.edu

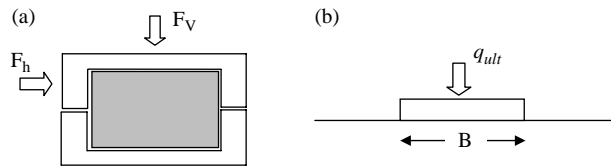


Figure 1. Schematic illustration of (a) direct shear box test and (b) footing load test.

that smaller samples exhibit higher strength. It is noted that the ASTM standard test method for direct shear testing requires a minimum specimen thickness H of six times the maximum particle diameter and a minimum specimen width L of 10 times the maximum particle diameter, in determining which shear box size should be used for testing sands. The minimum specimen width to thickness ratio, L/H , shall be 2:1. However, all the tests by Hight and Leroueil's (2003) meet these criteria, but the tests still result in large variation of friction angles.

For the case of a shallow strip footing on the surface of a cohesionless granular material as shown in Figure 1(b), the ultimate pressure q_{ult} required to cause instability, commonly used in shallow foundation design, is derived based on either the elastic–plastic model of Drucker–Prager or limit analysis (Terzaghi 1943, Meyerhof 1951, Hansen 1961). Both results give the following form:

$$q_{ult} = \frac{1}{2} N_\gamma \gamma B \quad \text{or} \quad N_\gamma = \frac{q_{ult}}{\gamma B/2}, \quad (1)$$

where B is the footing width and γ is the unit weight of soil. The dimensionless constant, N_γ , is only a function of material property, independent of footing size. Experimental measurements show that, for a given material, the value of N_γ is nearly a constant for large size footings. However, for small-scale experimental footing tests, the results have shown otherwise. In order to have a general

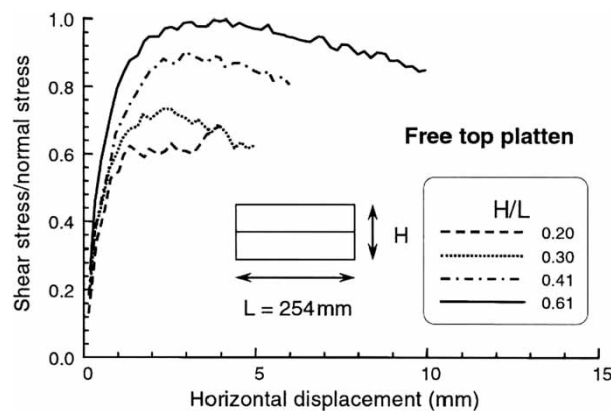


Figure 2. Influence of shear box aspect ratio on the friction angle (Hight and Leroueil 2003).

idea of the footing size effect, a collection of footing test results are plotted in Figure 3 for various types of sand. The results show that, for the same sand, the value of N_γ can be many times higher for a smaller footing size. The value of N_γ increases as the footing size B increases. For large footing sizes, the value of N_γ can be regarded as a constant.

The experimental results, both from shear box test and from footing tests, clearly demonstrated that the shear strength of sand has a scale effect, which is a contradiction to the common concept of dimension analysis in continuum mechanics.

3. Model formulation

In order to model the scale effect of granular material, a stress–strain law with internal length should be considered. For this purpose, the class of models for strain-gradient continuum can be adopted. The strain-gradient models treat that stress is a function of not only strain but also strain-gradient. The material constant that links the relationship between stress and strain-gradient contains a length scale, which is considered an intrinsic material property, and termed as *internal length* of the material. Within the strain-gradient models, there are two different approaches; the first approach considers only Cauchy stress, thus the work done is expressed by the traditional expression $\sigma_{ij} \Delta \varepsilon_{ij}$. The second approach considers an additional higher order stress μ_{ij} (conjugate to the strain-gradient $\Delta \chi_{ij}$), thus the work done is in a combined form of $\sigma_{ij} \Delta \varepsilon_{ij} + \mu_{ij} \Delta \chi_{ij}$.

The first approach is more popularly adopted because it is easier to implement. Without additional stress variables, its finite element formulation is only slightly varied from the traditional formulation. This approach has been recently employed by many researchers (DeBorst and

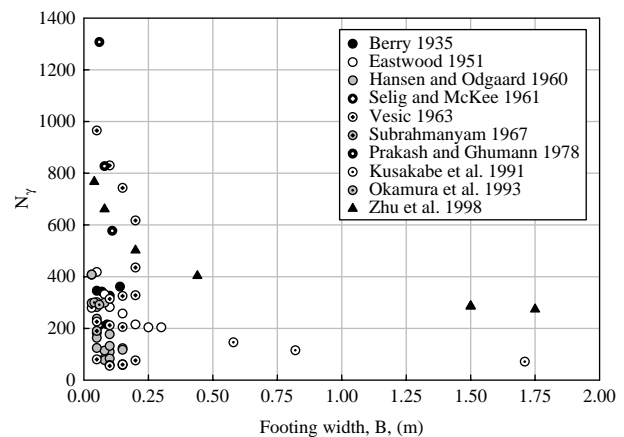


Figure 3. Results of model and prototype footing tests compiled from the literature (Berry 1935, Eastwood 1951, Hansen and Odgaard 1960, Selig and McKee 1961, Vesić 1963, Subrahmanyam 1967, Prakash and Ghumann 1978, Okamura et al. 1993, Kusakabe 1995, Zhu et al. 1998).

Muhlhaus 1992, Pamin 1994, Chang and Gao 1995, Peerling *et al.* 1996, Altan and Aifantis 1997, Aifantis 1999, Suiker *et al.* 2001, Abu Al-Rub and Voyiadjis 2004, Voyiadjis and Abu Al-Rub 2005, etc). On the other hand, the second approach is more rigorous because it includes strain-gradients and their conjugated higher order stresses under strict thermodynamics constraints (Chang *et al.* 2002). As a result, the finite element analysis is more robust. However, its finite element implementation is not a straightforward task.

Among various strain-gradient models of the second approach, the simplest but rigorous one is the 'couple stress solid' that utilises only the first gradient of rigid body rotation (see Mindlin and Tiersten 1962, Toupin 1962, Fleck and Hutchinson 1997, among others). As it is the simplest model suitable for particle rotation modelling, it is adopted in this paper. Here, the von Mises model used by Fleck and Hutchinson (1997) for metal is extended to Drucker-Prager model for frictional sand. A brief description is given below.

3.1 Generalised strains and stresses

For the couple-stress model, in addition to the usual strain (as the symmetric-part of displacement gradient), the rotation of particle ω_k is also introduced as a kinematic variable. The rotation in general is a variable independent of displacement (see Eringen 1968). However, in this couple-stress model, the rotation is assumed equal to the skew-part of displacement gradient

$$\varepsilon_{ij} = \frac{1}{2} \left(\frac{\partial u_i}{\partial x_j} + \frac{\partial u_j}{\partial x_i} \right); \quad \omega_j = \frac{1}{2} e_{jpk} \frac{\partial u_p}{\partial x_k} \quad (2)$$

Thus, the rotation gradient,

$$\chi_{ij} = \frac{\partial \omega_j}{\partial x_i} = \frac{1}{2} e_{jpk} \frac{\partial^2 u_p}{\partial x_k \partial x_i} \quad (3)$$

is the second derivative of displacement, and the model can be classified as a strain-gradient continuum. Corresponding to the strain ε_{ij} and strain-gradient χ_{ij} , the generalised stress includes Cauchy stress σ_{ij} and couple stress μ_{ij} . The work done per unit volume of the solid is $\Delta W = \sigma_{ij} \Delta \varepsilon_{ij} + \mu_{ij} \Delta \chi_{ij}$.

3.2 Equilibrium equation and boundary conditions

The couple stress plays a role in the equilibrium equation:

$$\frac{1}{2} e_{jpk} \frac{\partial^2 \mu_{ij}}{\partial x_k \partial x_p} - \frac{\partial \sigma_{iq}}{\partial x_i} = 0, \quad (4)$$

where the body force is neglected. The moment traction on the surface of the body is $q_j = \mu_{ij} n_i$, and the stress traction

is $\tau_q = \sigma_{qj} n_j - (1/2) e_{jpk} (\partial \mu_{ij} / \partial x_k) n_p$. The boundary conditions can be specified using the displacement u_k or the rotation ω_k .

3.3 Constitutive equations

3.3.1 Elastic stress-strain relationship

Besides the usual relationship between stress and strain, an additional relationship between couple stress and rotation gradient is required

$$\Delta \sigma_{ij} = C_{ijkl} \Delta \varepsilon_{kl}^e; \quad \Delta \mu_{ij} = D_{ijkl} \Delta \chi_{kl}^e \quad (5)$$

For a 2D condition, the constitutive matrix [C] contains the usual Lamé constants λ and G

$$[C] = \begin{bmatrix} \lambda + 2G & \lambda & 0 \\ \lambda & \lambda + 2G & 0 \\ 0 & 0 & G \end{bmatrix} \quad (6)$$

The constitutive matrix [D] contains the bending stiffness, κ . Evaluation of the bending stiffness will be described in the later section:

$$[D] = \begin{bmatrix} \kappa & 0 \\ 0 & \kappa \end{bmatrix} \quad (7)$$

3.3.2 Elastic-plastic stress-strain relationship

From strain-gradient plasticity theory developed by Fleck and Hutchinson (1997), the strain energy density w of a solid is taken to depend upon the second invariant of deviatoric strain, $\bar{\varepsilon}$, and the second invariant of the rotation gradient, $\bar{\chi}$. The overall effective strain $\bar{\Xi}$ is defined as

$$\bar{\Xi} = \sqrt{\bar{\varepsilon}^2 + l_{int}^2 \bar{\chi}^2}, \quad \text{where } \bar{\varepsilon} = \sqrt{\frac{2}{3}} e_{ij} e_{ij} \quad \text{and} \quad \bar{\chi} = \sqrt{\frac{2}{3}} \chi_{ij} \chi_{ij} \quad (8)$$

where l_{int} is the material internal length, e_{ij} is the strain deviator tensor and χ_{ij} is the rotation gradient tensor.

Similarly, the overall effective stress $\bar{\Sigma}$ is defined as a function of the second invariant of deviatoric stress, $\bar{\sigma}$, and the second invariant of the couple stress μ_e , which is expressed as

$$\bar{\Sigma} = \sqrt{\bar{\sigma}^2 + l_{int}^2 \bar{\mu}^2}, \quad \text{where} \quad (9)$$

$$\bar{\sigma} = \sqrt{\frac{3}{2}} s_{ij} s_{ij} = \sqrt{3J_2}, \quad \text{and} \quad \bar{\mu} = \sqrt{\frac{3}{2}} \mu_{ij} \mu_{ij},$$

where s_{ij} is the stress deviator tensor, μ_{ij} is the couple-stress tensor and $J_2 = (1/2) s_{ij} s_{ij}$.

The general expression of a yield surface for a work-hardening/softening material has the form

$$f(\sigma_{ij}, \varepsilon_{ij}^p, k) = 0, \quad (10)$$

where $k = k(\Xi^p)$ is a hardening/softening parameter. Ξ^p is the effective plastic strain.

To include the effects of hydrostatic stress on the shearing resistance of the material, the modified von Mises yield function (Drucker and Prager 1952) was adopted,

$$f = \Sigma - k(\Xi^p) + \sqrt{3}\beta p = 0, \quad (11)$$

where Σ and Ξ^p are defined in Equations (8) and (9), $p = (\sigma_1 + \sigma_2 + \sigma_3)/3 = I_1/3$ is the mean stress and β is the friction-like parameter. Here, for soil, stress operates at the compression range. Hence, positive p indicates compression and this term should be positive as in Equation (11). Figure 4 depicts the Drucker–Prager yield surface in the $\Sigma - I_1$ surface.

The parameters, k and β , can be determined from failure stress data which usually are expressed in terms of cohesion c and frictional angle ϕ of the material. For tri-axial compression, the relations are

$$\beta = \frac{6 \sin \phi}{(3 - \sin \phi)}; \quad k = c \frac{6 \cos \phi}{(3 - \sin \phi)}. \quad (12)$$

When plane strain conditions are warranted, the material constants β and k are related to ϕ and c by

$$\beta = \frac{3 \tan \phi}{\sqrt{9 + 12 \tan^2 \phi}}; \quad k = \frac{3\sqrt{3}c}{\sqrt{9 + 12 \tan^2 \phi}}. \quad (13)$$

For simplicity, a linear strain-softening yield function is applied in the analysis, which is shown in Figure 5.

The material yields at stress Σ_y and has a softening modulus h . A small residual strength Σ_r is specified to avoid the occurrence of unrealistic negative stresses due to extrapolation of the linear relationship at large strain.

Associated flow rule is assumed, which stipulates the plastic potential function $g = f$. The flow rule is defined as

$$d\Xi^p = d\lambda \frac{\partial f}{\partial \Sigma}, \quad (14)$$

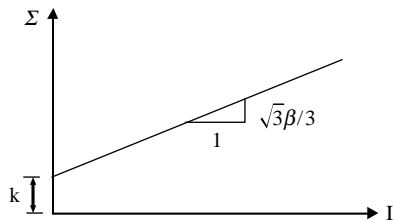


Figure 4. Drucker–Prager yield surface in the $\Sigma - I$ plane.

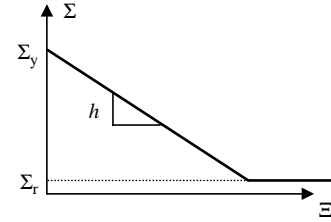


Figure 5. Linear strain-softening function.

where $d\lambda$ is a non-negative scalar function that will determine the magnitude of the plastic flow. The elastic–plastic stress–strain relationship based on the yield function and flow rule is derived in Appendix.

3.4 Finite element formulation

Implementation of the couple-stress model into a standard finite element code is not straightforward. Only a few finite element formulations exist in the literature for couple stress solids. Ristinmaa and Vecchi (1996) used a C^1 continuous shape function that guarantees continuous displacement gradients at nodal points. On the other hand, Xia and Hutchinson (1996) and Shu *et al.* (1999) used a C^0 shape function by treating rotation and displacement as two independent variables. Then, a Lagrange multiplier was used to enforce the constraint between displacement gradient and rotation. Unfortunately, convergence of the finite element formulation with two kinematic fields is conditional to the orders of the selected shape functions for displacement and rotation (Hughes and Brezzi 1989). For this reason, a modified variational formulation was proposed to render unconditional convergence (Chang and Shi 2005). We have adopted this approach to implement the elasto-plastic model in the finite element method.

4. Internal length

Internal length is the key parameter that makes the model capable of simulating scale effect. A mathematical definition of particle internal length was presented by Chang and Shi (2005) as the ratio of inter-particle rolling stiffness to the inter-particle compressive stiffness. The rolling resistance is influenced by many factors. For instance, particles with flat contact surface give higher rolling resistance. The arrangement of neighbouring particles also contributes to the rolling resistance. Thus, internal length is related to particle shape, degree of interlocking and binder stiffness. Angular particles generally have a high degree of interlocking and therefore, a higher internal length. On the other hand, the round particles generally exhibit a lower internal length. However, at this time, the factors influencing internal

length cannot be separated and quantified, thus internal length cannot be determined directly from microscale information. It can only be phenomenologically determined by comparison with experimental results. In a later section, we will evaluate the values of internal length for real sands.

When subjected to deformation, moments transmit between particles in the system. The presence of such moments, neglected in the classic continuum, can be better described by a couple-stress medium, in which an additional relationship between couple stress and rotational gradients is provided. As shown in Equations (5) and (7), parameter κ governs the magnitudes of moment transmit between particles. It has been shown from a micromechanics derivation (Chang *et al.* 2003) that the bending stiffness, κ , can be expressed as

$$\kappa = \frac{E}{1 - \nu} l_{\text{int}}^2, \quad (15)$$

where E is the elastic modulus, ν is the Poisson's ratio and κ is the bending modulus. When internal length is zero, the couple stress becomes null. Thus, it reduces the material to a classic continuum. For angular aggregates, the internal length will facilitate a large moment transmitting within the material.

It is noted that moment can be transmitted in the material through two modes: through contact-forces and through contact-moments between particles. For a large sample size, a large length of moment arm is involved; thus, the moments are dominant by the contact forces. On the other hand, for a small scale, the moments are dominant by contact moments. Therefore, scale effect exhibits in a footing test, or in a shear box test.

Parameters required for the model are cohesion c , friction angle ϕ , Young's modulus E and Poisson ratio ν , hardening/softening parameter h and internal length l_{int} . In this paper, we aim to study how the consideration of internal length alone will affect the traditional bearing capacity solution, which is based on a perfect plastic Drucker–Prager model. Therefore, the softening parameter h is assigned a number negligibly small to represent the perfect plastic condition.

5. Finite element analyses

5.1 Finite element analysis for direct shear experiments

The finite element simulations for direct shear box tests were performed in the same manner as the experimental tests. Two shear box sizes (63.5 and 101.6 mm) were used in the simulation. Figures 6 and 7 show the mesh used in the simulations. The confining stress was applied as a uniform pressure downward in the vertical direction.

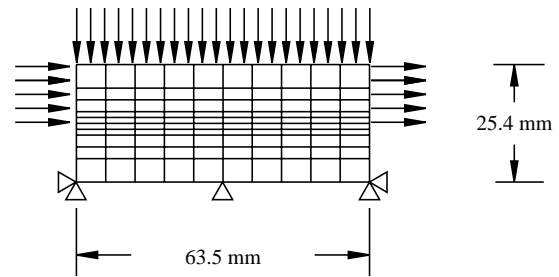


Figure 6. Finite element mesh for direct shear box (63.5 mm).

The bottom of the box was fixed in both directions. The sides of lower half box were fixed in the x direction, allowing the specimen to consolidate vertically. The top half of the box was displaced as a rigid box by specifying the same displacement magnitudes on both sides. This simulated the rigid metal box movement in the experimental test. The shear strength was taken at a displacement of 10% of the box width to be consistent with experimental tests. Seven different normal stresses were used to capture the curvature of the Mohr–Coulomb failure envelope: 6.9, 34.5, 68.9, 103.4, 137.9, 172.4 and 517.1 kPa (1, 5, 10, 15, 20, 25 and 75 psi). These normal stresses were similar to those used in the experimental programme.

5.2 Finite element analysis for footing test

The mesh dimensions and boundary conditions of the problem are designated in Figure 8. Because of the symmetrical condition, Figure 8 reveals only the right half of the complete footing problem. The dimensions of the steel box with the concrete base match with those of the model-scale footing test; $H = 0.30$ m, $L = 0.46$ m (half the box length) and $B = 50.8$ mm. Soil gravity was considered in this analysis. At the base, the displacements were specified to be zero in the x and y directions and the displacements on the left-side wall was specified to be zero in the x direction and in both the x and y directions on the right-side wall. A plane strain condition was applied. Here, associative flow rule is used for simplicity and for comparison with classic solutions.

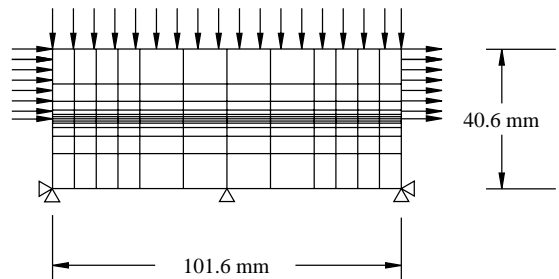


Figure 7. Finite element mesh for direct shear box (101.6 mm).

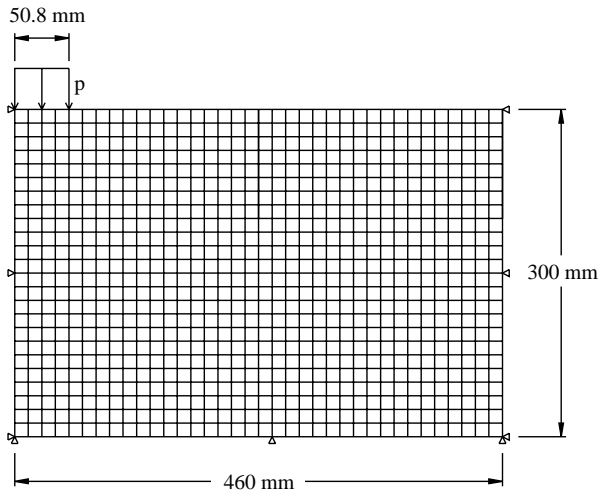


Figure 8. Finite element mesh for footing analysis.

6. Comparison between prediction and experiments

6.1 Soils used in experiments

The tests results used for comparison were selected from the work by Cerato (2005). Results for two sands were selected brown mortar sand and winter sand. The gradation curves for the two sands are shown in Figure 9. Brown mortar sand is uniformly graded (i.e. the particle size distribution is narrow), whereas winter sand is well graded. The ratio D_{60}/D_{10} is 2.1 and 4.5, respectively. The values of D_{50} are very close for the two sands; $D_{50} = 0.6$ mm for brown mortar sand and $D_{50} = 0.7$ mm for winter sand. The loosest and densest states of the two sands were determined in accordance with ASTM standard tests. For brown mortar sand, $e_{min} = 0.58$ and $e_{max} = 0.91$ and for winter sand, $e_{min} = 0.37$ and $e_{max} = 0.67$. It is easier to compact winter sand to a higher density. The aspect ratios for both sands are about the same, 1.32–1.33. The roundness is 0.79 for brown mortar sand and 0.34 for winter sand, indicating that particle shapes of the two

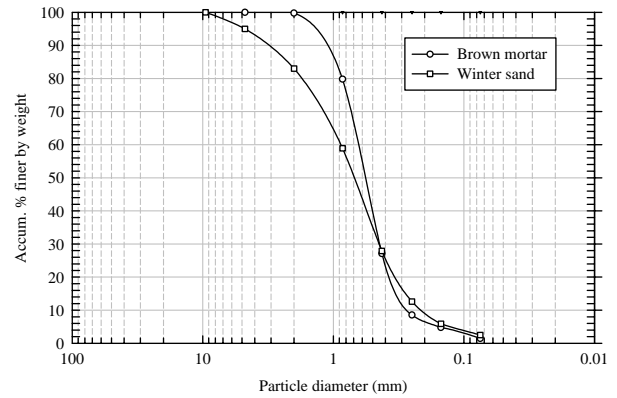


Figure 9. Gradation curves for brown mortar sand and winter sand.

sands are distinctly different. Based on the roundness criterion given by Powers (1953), brown mortar sand is well rounded and winter sand is subangular. It is, therefore, expected that these two sands would have different magnitudes of *internal length*.

6.2 Direct shear test simulations

In the direct shear box test simulations, the finite element predictions are performed for dense soils (relative density $D_r = 70\%$ for brown mortar sand and 87% for winter sand) tested in two box sizes: 63.5 and 101.6 mm. The predictions and experimental data are plotted in Figure 10. Due to the high density of winter sand, the measured friction angles are higher than those of brown mortar sand, Figure 10.

In the prediction, internal length is specified as 2.54 and 25.4 mm, respectively, for brown mortar sand and winter sand. Other input parameters are given in Table 1. The values of cohesion are negligibly small, thus are not listed.

For the two different sizes of shear box, the friction angle in general varies about $4\text{--}10^\circ$ for the winter sand,

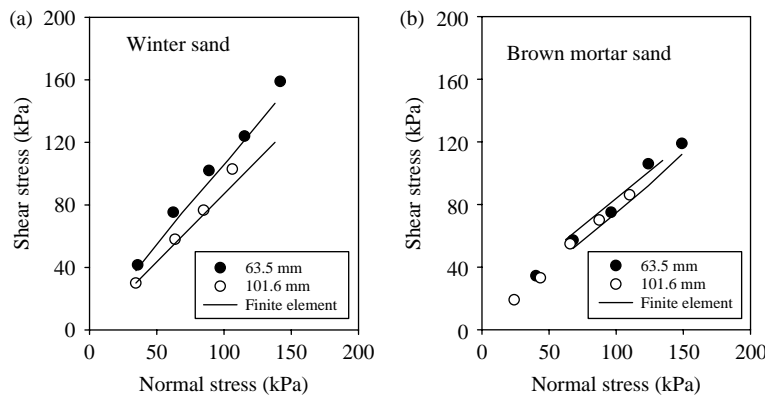


Figure 10. Comparison of predicted and measured direct shear box results for two different types of sand.

Table 1. Input parameters in finite element simulation for direct shear box tests.

	ϕ	E	ν	l_{int}
Brown mortar sand	37°	13.8 MPa	0.3	2.54 mm
Winter sand	45°	13.8 MPa	0.3	25.4 mm

but varies little in the brown mortar sand. The variation of friction angle is plotted in terms of shear box size (see Figure 11). For easy comparison purposes, it is also plotted in a normalised form with ϕ/ϕ_B in the vertical axis, where ϕ_B is the estimated friction angle when box size is infinity (here we use 45° for winter sand and 37° for brown mortar sand).

In Figure 11, both sands show change in friction angle with box size. However, a more significant change in friction angle is observed for winter sand. This behaviour can be modelled using a larger internal length for winter sand, because a larger internal length gives more pronounced friction angle change with box size. Internal lengths between 2.54 and 25.4 mm seem to bracket the two different sands used in the study. This difference in internal length is attributed primarily to the influence of particle shape. The well round brown mortar sand has less ability of transmitting moment between particles than winter sand, which has subangular particles.

The thickness of shear zone (shear band) is not easy to depict from experiments. However, it can be observed from the shear strain profile obtained in the finite element simulation. The thickness of shear zone in the winter sand is larger than that in the brown mortar sand. The thickness of shear zone has been experimentally observed as a function of particle size as indicated by Palmeira and Milligan (1989) for Leighton Buzzard Sand in a small, medium and large shear box. Figure 12 shows the ratio between the shear zone thickness and the sample height (t/H), which is plotted against the sample height to mean particle diameter ratio (H/D_{50}) for several tests with

Leighton Buzzard Sand. This figure shows that the thickness of the shear zone decreases for small particle size if the specimen size remains the same. The thickness of shear zone is plotted in Figure 12 for brown mortar sand and for winter sand. The points are positioned on the vicinity of the trend curve. The ratio of thickness of shear zone (t/H) is larger for the smaller box size. The particle size is not the only influencing factor; the particle shape can also significantly affect the thickness of shear zone.

6.3 Bearing capacity

The experimental measurements for sand in the range from medium dense to dense are plotted in Figure 13. The experimental data show that N_γ is strongly dependent on footing size (Cerato 2005). As footing size increases, the value of N_γ decreases and finally converges to a constant $N_{\gamma B}$. The value of $N_{\gamma B}$ is 80 for winter sand and 350 for brown mortar sand. In Figure 13, the symbols are the measured experimental results, and the solid lines are the predictions from finite element model. In the finite element analyses, the input material parameters for brown mortar sand and winter sand are given in Table 2.

It is noted that the input parameters in Table 2 are the same as those in Table 1 except for the friction angles. In the previous case, the two sand specimens used in the direct shear box tests had specific densities. The footing test results are shown in Figure 13; however, were measured from sand with a range of densities. Thus in Table 2, the average friction angles are estimated to represent the soils with this range of densities. The same values of internal lengths were kept to show the same effect of particle shapes. Figure 13 shows a good agreement between measured and predicted trends, which is due to footing size effect.

In order to compare the effect of footing size, the data are replotted in Figure 14 on a normalised scale. It can be

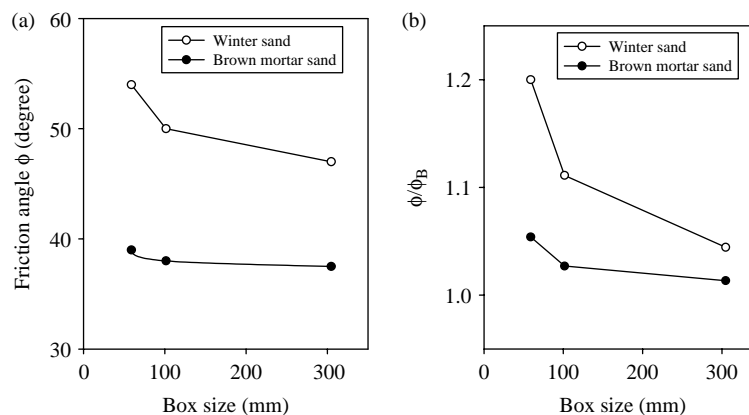


Figure 11. The effect of shear box size on friction angle.

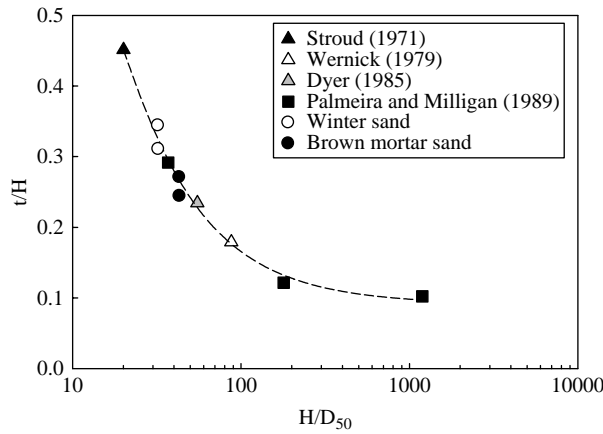


Figure 12. Influence of scale on shear zone thickness after Palmeira and Milligan (1989): Stroud (1971), Wernick (1979), Dyer (1985), winter sand, brown mortar sand

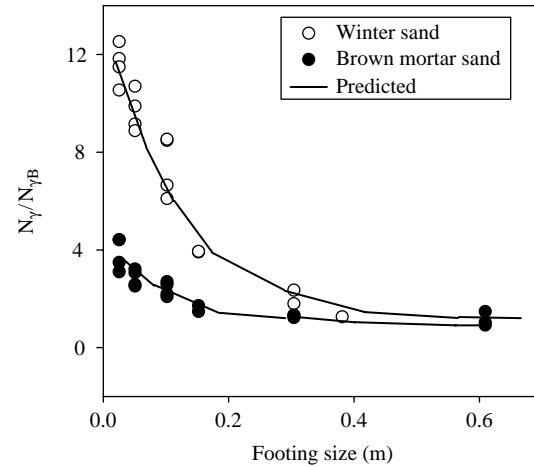


Figure 14. The effect of footing size on N_γ .

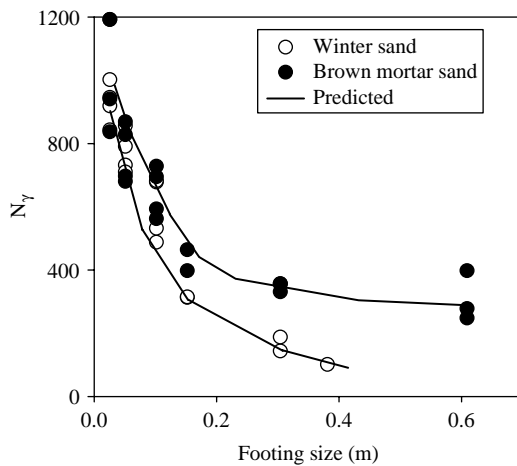


Figure 13. Comparison between predicted and measured bearing capacity for two different types of sands.

Table 2. Input parameters in finite element simulation for footing tests.

	ϕ	E	ν	l_{int}
Brown mortar sand	44°	13.8 MPa	0.3	2.54 mm
Winter sand	37°	13.8 MPa	0.3	25.4 mm

seen that the footing size has a smaller influence on the bearing capacity for brown mortar sand than for winter sand. This is expected because of its well round particles and its smaller resistance to rotation through inter-particle contacts.

7. Conclusion

The scale effect is a fundamental problem of considerable importance to soil mechanics. A couple-stress model has

been investigated for the scale effect on shear strength of sands. In the couple-stress model, by considering the relationship between rotation gradient and couple stress, the rolling resistance between particles is explicitly considered as a contribution to the overall shear strength. This part of contribution only becomes significant when the size of the problem is relatively small. Therefore, for a small size shear box or footing, higher shear strength is observed. On the other hand, this part of the contribution is insignificant when the size of the problem is relatively large. Therefore, the problem of large footing size can be analysed using the conventional model.

In the couple-stress model, the key material parameter is internal length, which shows the degree of rolling resistance of the material. The overall contribution to shear strength depends on the ratio of internal length to the problem size (i.e. l_{int}/B , where B can be taken as the footing size or the shear box size). When this ratio approaches zero, the present model reduces to the classic Drucker–Prager plasticity model. The degree of scale effect can be captured by this model with different magnitudes of internal length.

The value of internal length for sand is evaluated from the experimental tests from the literature and from the tests carried out by Cerato (2005). On the basis of the finite element analyses, the internal length is approximately 2.5 mm for sand with round particles and 25 mm for sand with angular particles. This range seems to predict results that bracket the experimentally measured data for brown mortar sand and winter sand.

References

Abu Al-Rub, R.K. and Voyiadjis, G.Z., 2004. Analytical and experimental determination of the material intrinsic length scale of strain gradient plasticity theory from micro- and nano-indentation experiments. *International Journal of Plasticity*, 20 (6), 1139–1182.

- Aifantis, E.C., 1999. Gradient deformation models at nano, micro, and macro scales. *Journal of Engineering Materials and Technology*, 121, 189–202.
- Altan, B.S. and Aifantis, E.C., 1997. On some aspects in the special theory of gradient elasticity. *Journal of the Mechanical Behavior of Materials*, 8, 231–282.
- Atkinson, M., 1995. Further analysis of the size effective in indentation hardness tests of some metals. *Journal of Material Resources*, 10, 2908–2915.
- Bandis, S., 1979. *Experimental studies on shear strength-size relationships and deformation characteristics of rock discontinuities*. Dissertation (PhD). University of Leeds.
- Bazant, Z.P., 2000. Size effect. *International Journal of Solids and Structures*, 37, 69–80.
- Berry, D.S., 1935. Stability of granular mixtures – American Society for Testing Materials. *Proceedings of the 38th Annual Meeting*, 35 (2), 491–507.
- Cerato, A.B., 2005. *Scale effect of shallow foundation bearing capacity on granular material*. Dissertation (PhD). University of Massachusetts, Amherst.
- Chang, C.S. and Gao, J., 1995. Second-gradient constitutive theory for granular material with random packing structure. *International Journal of Solids and Structures*, 32 (16), 2279–2293.
- Chang, C.S. and Shi, Q., 2005. A mix-mode elastic finite element formulation for bonded granular material considering rotation of particles. *Journal of Engineering Mechanics*, 131 (2), 120–130.
- Chang, C.S., Askes, H., and Sluys, L.J., 2002. Higher-order strain/higher-order stress gradient models derived from a discrete microstructure, with application to fracture. *Engineering Fracture Mechanics*, 69, 1907–1924.
- Chang, C.S., Shi, Q., and Liao, C.L., 2003. Elastic constants for granular materials modeled as first-order strain-gradient continua. *International Journal of Solids and Structures*, 40, 5565–5582.
- DeBeer, E.E., 1965. The scale effect on the phenomenon of progressive rupture in cohesionless soils. *Proceedings of the Sixth International Conference on Soil Mechanics and Foundation Engineering*, 2 (3–6), 13–17.
- DeBorst, R. and Mühlhaus, H.-B., 1992. Gradient-dependent plasticity: formulation and algorithmic aspects. *International Journal for Numerical Methods in Engineering*, 35 (5), 21–39.
- Drucker, D.C. and Prager, W., 1952. Soil mechanics and plastic analysis of limit design. *Quarterly Journal of the Applied Mathematics*, 10 (2), 157–165.
- Eastwood, W., 1951. A comparison of the bearing power of footings on dry and inundated sand. *The Structural Engineer: The Journal of the Institution of Structural Engineers*, 29 (1), 1–11.
- Eringen, A.C., 1968. Theory of micropolar elasticity. In: H. Liebowitz, ed. *Fracture, an advance treatise*. New York: Academic Press.
- Fleck, N.A. and Hutchinson, J.W., 1997. Strain gradient plasticity. In: J.W. Hutchinson and T.Y. Wu, eds. *Advances in applied mechanics*. Vol. 33. New York: Academic Press, 295–361.
- Fleck, N.A., et al., 1994. Strain gradient plasticity: theory and experiment. *Acta Metallurgica et Materialia*, 42 (2), 475–487.
- Hansen, B., 1961. *A general formula for bearing capacity*. Bulletin 11. Copenhagen: Geoteknisk Institute.
- Hansen, B. and Odgaard, D., 1960. *Bearing capacity tests on circular plates on sand*. Bulletin No. 8. Denmark: The Danish Geotechnical Institute.
- Hight, D.W. and Leroueil, S., 2003. Characterisation of soils for engineering purposes. *Proceedings of the Characterisation and Engineering Properties of Natural Soils*, 1, 255–360.
- Hudson, J.A., 1993. Rock properties, testing methods and site characterization. In: J.A. Hudson, ed. *Comprehensive rock engineering*. Oxford: Pergamon, 1–39.
- Hughes, T.J.R. and Brezzi, F., 1989. On drilling degrees of freedom. *Computer Methods in Applied Mechanics and Engineering*, 72, 105–121.
- Hutchinson, J.W., 2000. Plasticity at the micron scale. *International Journal of Solids and Structures*, 37, 225–238.
- Kusakabe, O., 1995. Foundations. *Geotechnical centrifuge technology*. New York: Blackie, 179–186.
- Ma, Q. and Clarke, D.R., 1995. Size dependent hardness of silver single crystals. *Journal of Material Research*, 10, 853–863.
- Meyerhof, G.G., 1951. The ultimate bearing capacity of foundations. *Geotechnique*, 11 (4), 301–332.
- Mindlin, R.D. and Tiersten, H.F., 1962. Effect of couple stresses in linear elasticity. *Archive for Rational Mechanics and Analysis*, 11, 415–418.
- Okamura, M., Takemura, J., and Kimura, T., 1993. Study on bearing capacity of shallow footings on sand. *Proceedings of the Japanese Society of Civil Engineering*, No. 463, 85–94.
- Palmeira, E.M. and Milligan, G.W.E., 1989. Scale effects in direct shear tests on sand. *Proceedings of the 12th International Conference on Soil Mechanics and Foundation Engineering*, 1 (1), 739–742.
- Pamin, J., 1994. *Gradient-dependent plasticity in numerical simulation of localization phenomena*. Dissertation (PhD). Delft University of Technology.
- Parsons, J.D., 1936. Progress report on an investigation of the shearing resistance of cohesionless soils. *Proceedings of the 1st International Conference on Soil Mechanics and Foundation Engineering*, 2, 133–138.
- Peerling, R.H.J., et al., 1996. Gradient enhanced damage for quasi-brittle materials. *International Journal for Numerical Methods in Engineering*, 39 (3), 391–403.
- Poole, W.J., Ashby, M.F., and Fleck, N.A., 1996. Micro-hardness tests on annealed and work-hardened copper polycrystal. *Scripta Metallurgy Materials*, 34, 559–564.
- Powers, M.C., 1953. A new roundness scale for sedimentary particles. *Journal of Sedimentary Petrology*, 23 (2), 117–119.
- Prakash, S. and Ghumman, M.S., 1978. Effect of shape on bearing capacity of model footings in sand. *Journal of the Institution of Engineers (India). Civil Engineering Division* 59, 186–191.
- Ristinmaa, M. and Vecchi, M., 1996. Use of couple-stress theory in elasto-plasticity. *Computer Methods in Applied Mechanics and Engineering*, 136, 205–224.
- Selig, E.T. and McKee, K.E., 1961. Static and dynamic behavior of small footings. *Journal of the Soil Mechanics and Foundations Division, ASCE*, 87 (SM6), 29–47.
- Shu, J.Y., King, W.E., and Fleck, N.A., 1999. Finite element analysis of indentation – the role of micro length scale. *International Journal of Numerical Methods in Engineering*, 44, 373–391.
- Stroud, M.A., 1971. *The behavior of sand at low stress levels in the simple shear apparatus*. Thesis (PhD). University of Cambridge, England.

- Subrahmanyam, G., 1967. The effect of roughness of footings on bearing capacity. *Journal of the Indian National Society of Soil Mechanics and Foundation Engineering*, 6, 33–45.
- Suiker, A.S.J., deBorst, R., and Chang, C.S., 2001. Micro-mechanical modeling of granular material. Part 1 – derivation of a second-gradient micro-polar constitutive theory. *Acta Mechanica*, 149, 161–180.
- Tatsuoka, F., et al., 1991. Progressive failure and particle size effect in bearing capacity of a footing on sand. *Geotechnical Special Publication No. 27*, 2, 788–802.
- Terzaghi, K., 1943. *Theoretical soil mechanics*. New York: John Wiley and Sons, Inc.
- Toupin, R.A., 1962. Elastic materials with couple-stresses. *Archive for Rational Mechanics and Analysis*, 11, 385–414.
- Vesić, A.S., 1963. Bearing capacity of deep foundations in sand. *Highway Research Board (Annual Meeting)*.
- Voyiadjis, G.Z. and Abu Al-Rub, R.K., 2005. Gradient plasticity theory with a variable length scale parameter. *International Journal of Solids and Structures*, 42 (14), 3998–4029.
- Wernick, E., 1979. A true direct shear apparatus to measure soil parameters of shear bands. *Design Parameters in Geotechnical Engineering, British Geotechnical Society*, 2, 175–182.
- Xia, Z. and Hutchinson, J.W., 1996. Crack tip fields in strain gradient plasticity. *Journal of the Mechanics and Physics of Solids*, 44, 1621–1648.
- Zhu, F., Clark, J.I., and Phillips, R., 1998. Bearing capacity of ring foundations under vertical load. *Centrifuge* 98, 1, 441–446.

Appendix. Incremental elastic–plastic stress–strain formulation

In this appendix, the incremental formulation for the elastic–plastic stress–strain relationship is derived. The total strain increment is assumed as the sum of the elastic strain increment and the plastic strain increment. In a gradient plasticity, the yield strength of the solid is taken to depend upon both strain ε and the rotation gradient χ . Therefore, the increment of rotation gradient is also divided into elastic and plastic part

$$\begin{Bmatrix} d\varepsilon_{ij} \\ d\chi_{ij} \end{Bmatrix} = \begin{Bmatrix} d\varepsilon_{ij}^e \\ d\chi_{ij}^e \end{Bmatrix} + \begin{Bmatrix} d\varepsilon_{ij}^p \\ d\chi_{ij}^p \end{Bmatrix}, \quad (16)$$

From Hooke’s law, the stress increment can be expressed as

$$\begin{Bmatrix} d\sigma_{ij} \\ d\mu_{ij} \end{Bmatrix} = \begin{bmatrix} C_{ijkl} & 0 \\ 0 & D_{ijkl} \end{bmatrix} \begin{Bmatrix} d\varepsilon_{kl}^e \\ d\chi_{kl}^e \end{Bmatrix} = \begin{bmatrix} C_{ijkl} & 0 \\ 0 & D_{ijkl} \end{bmatrix} \begin{Bmatrix} (d\varepsilon_{kl} - d\varepsilon_{kl}^p) \\ (d\chi_{kl} - d\chi_{kl}^p) \end{Bmatrix}, \quad (17)$$

where C_{ijkl} is the tensor of lower order elastic stiffness and D_{ijkl} is the tensor of higher order elastic stiffness. The plastic strain increment is obtained from the flow rule

$$\begin{Bmatrix} d\varepsilon_{ij}^p \\ d\chi_{ij}^p \end{Bmatrix} = d\lambda \begin{Bmatrix} \frac{\partial f}{\partial \sigma_{ij}} \\ \frac{\partial f}{\partial \mu_{ij}} \end{Bmatrix}. \quad (18)$$

Then, the stress–strain relations for a work-hardening/softening material are expressed as

$$\begin{Bmatrix} d\sigma_{ij} \\ d\mu_{ij} \end{Bmatrix} = \begin{bmatrix} C_{ijkl} & 0 \\ 0 & D_{ijkl} \end{bmatrix} \begin{Bmatrix} (d\varepsilon_{kl} - d\lambda \frac{\partial f}{\partial \sigma_{kl}}) \\ (d\chi_{kl} - d\lambda \frac{\partial f}{\partial \mu_{kl}}) \end{Bmatrix}. \quad (19)$$

During plastic deformation, the stress point stays on the yield surface. The consistency condition for a general work-hardening or softening material is

$$df = \begin{bmatrix} \frac{\partial f}{\partial \sigma_{ij}} & \frac{\partial f}{\partial \mu_{ij}} \end{bmatrix} \begin{Bmatrix} d\sigma_{ij} \\ d\mu_{ij} \end{Bmatrix} + \begin{bmatrix} \frac{\partial f}{\partial \varepsilon_{ij}^p} & \frac{\partial f}{\partial \chi_{ij}^p} \end{bmatrix} \begin{Bmatrix} d\varepsilon_{ij}^p \\ d\chi_{ij}^p \end{Bmatrix} = 0. \quad (20)$$

Substituting Equation (18) into Equation (20) and solving we get

$$d\lambda = \frac{1}{H} \left(\frac{\partial f}{\partial \sigma_{ij}} C_{ijkl} d\varepsilon_{kl} + \frac{\partial f}{\partial \mu_{ij}} D_{ijkl} d\chi_{kl} \right), \quad (21)$$

where

$$H = \frac{\partial f}{\partial \sigma_{ij}} C_{ijkl} \frac{\partial f}{\partial \sigma_{kl}} + \frac{\partial f}{\partial \mu_{ij}} D_{ijkl} \frac{\partial f}{\partial \mu_{kl}} - \frac{\partial f}{\partial \varepsilon_{ij}^p} \frac{\partial f}{\partial \sigma_{ij}} - \frac{\partial f}{\partial \chi_{ij}^p} \frac{\partial f}{\partial \mu_{ij}}. \quad (22)$$

Using Equations (17) and (21), the stress increment can be calculated from a given strain increment. The relationship is

$$\begin{Bmatrix} d\sigma_{ij} \\ d\mu_{ij} \end{Bmatrix} = \begin{bmatrix} C_{ijkl} & 0 \\ 0 & D_{ijkl} \end{bmatrix} \times \left\{ \begin{Bmatrix} (d\varepsilon_{kl} - \frac{1}{H} \left(\frac{\partial f}{\partial \sigma_{ij}} C_{ijkl} d\varepsilon_{kl} + \frac{\partial f}{\partial \mu_{ij}} D_{ijkl} d\chi_{kl} \right) \frac{\partial f}{\partial \sigma_{kl}}) \\ (d\chi_{kl} - \frac{1}{H} \left(\frac{\partial f}{\partial \sigma_{ij}} C_{ijkl} d\varepsilon_{kl} + \frac{\partial f}{\partial \mu_{ij}} D_{ijkl} d\chi_{kl} \right) \frac{\partial f}{\partial \mu_{kl}}) \end{Bmatrix} \right\}. \quad (23)$$

With some mathematical manipulation, the incremental stress–strain relationships are expressed as

$$\begin{Bmatrix} d\sigma_{ij} \\ d\mu_{ij} \end{Bmatrix} = [C^{ep}] \begin{Bmatrix} d\varepsilon_{kl} \\ d\chi_{kl} \end{Bmatrix}, \quad (24)$$

where the matrix

$$[C^{ep}] = \begin{bmatrix} C_{ijkl} - \frac{1}{H} C_{ijmn} \frac{\partial f}{\partial \sigma_{mn}} \frac{\partial f}{\partial \sigma_{pq}} C_{pqkl} & -\frac{1}{H} C_{ijmn} \frac{\partial f}{\partial \sigma_{mn}} \frac{\partial f}{\partial \sigma_{pq}} D_{pqkl} \\ -\frac{1}{H} D_{ijmn} \frac{\partial f}{\partial \sigma_{mn}} \frac{\partial f}{\partial \sigma_{pq}} C_{pqkl} & D_{ijkl} - \frac{1}{H} D_{ijmn} \frac{\partial f}{\partial \sigma_{mn}} \frac{\partial f}{\partial \sigma_{pq}} D_{pqkl} \end{bmatrix}. \quad (25)$$